AFRL-RV-HA-TR-2008-1138

Development of Data Analysis Techniques to Provide Photometric Images for a Heliospheric Imager

Bernard V. Jackson
Andrew Buffington
P. Paul Hick

University of California, San Diego
9500 Gilman Drive
La Jolla, CA 92093

Final Report

31 Oct 2008

AIR FORCE RESEARCH LABORATORY
Space Vehicles Directorate
29 Randolph Road
AIR FORCE MATERIEL COMMAND
HANSCOM AFB, MA 01731-3010

This technical report has been reviewed and is approved for publication.

AFRL-RV-HA-TR-2008-1138

/ signed /	/ signed /
JANET C. JOHNSTON	DWIGHT T. DECKER, Chief
Contract Manager	Space Weather Center of Excellence

REPORT DOCUMENTATION PAGE

Form Approved
OMB No. 0704-01-0188

PLEASE DO NOT RETURN YOUR FORM TO THE ABOVE ADDRESS.

1. REPORT DATE *(DD-MM-YYYY)*	2. REPORT TYPE	3. DATES COVERED *(From - To)*
31-10-2008	Scientific, Final	16-06-2004 – 30-09-2008

4. TITLE AND SUBTITLE

Development of Data Analysis Techniques to Provide Photometric Images for a Heliospheric Imager

5a. CONTRACT NUMBER
FA8718-04-C-0050

5b. GRANT NUMBER

5c. PROGRAM ELEMENT NUMBER
63401F

6. AUTHORS

Bernard V. Jackson
Andrew Buffington
P. Paul Hick

5d. PROJECT NUMBER
5021

5e. TASK NUMBER
RD

5f. WORK UNIT NUMBER
A1

7. PERFORMING ORGANIZATION NAME(S) AND ADDRESS(ES)

The Regents of the University of California, San Diego
9500 Gilman Drive
La Jolla, CA 92083

8. PERFORMING ORGANIZATION REPORT NUMBER

9. SPONSORING/MONITORING AGENCY NAME(S) AND ADDRESS(ES)

Air Force Research Laboratory /RVBXS
29 Randolph Road
Hanscom AFB, MA 01731-3010

10. SPONSOR/MONITOR'S ACRONYM(S)
AFRL/RVBXS

11. SPONSOR/MONITOR'S REPORT NUMBER(S)
AFRL-RV-HA-TR-2008-1138

12. DISTRIBUTION/AVAILABILITY STATEMENT

Approved for Public Release; distribution unlimited.

13. SUPPLEMENTARY NOTES

14. ABSTRACT

The Solar Mass Ejection Imager (SMEI) spacecraft has shown that it is feasible to image the changing global electron content of the heliosphere. With this contract UCSD helped provide unique software algorithms for processing the SMEI flight data that are capable of obtaining heliospheric images at high spatial and temporal resolution from an 840 km Earth orbit. The imaging enhancements devised involved several new and unique state-of-the-art and never before attempted principles for SMEI operation. These include techniques to allow a CCD camera to provide differential photometry of 0.1% over the sky and especially at 90° from the Sun-Earth line. This unprecedented precision is required to image and model CMEs and other heliospheric structures as they move outward from the Sun and engulf Earth. With this contract we perfected the measurements required to register and normalize these images. Thus, with these analyses, the scientific capability of heliospheric imager systems have been validated and can be used to accurately track CMEs in three dimensions as well as assess their potential as a space weather forecast tool.

15. SUBJECT TERMS

Sun-Earth connection Coronal mass ejections Heliospheric plasma 3D tomography Zodiacal light Spaceborne optical instrument

16. SECURITY CLASSIFICATION OF:			17. LIMITATION OF ABSTRACT	18. NUMBER OF PAGES	19a. NAME OF RESPONSIBLE PERSON
a. REPORT	b. ABSTRACT	c. THIS PAGE			Janet C. Johnston
UNCL	UNCL	UNCL	UNL		19B. TELEPHONE NUMBER *(Include area code)*

Contents

FIGURES

TABLE

FOREWORD

Development of Data Analysis Techniques to Provide Photometric Images for a Heliospheric Imager

We launched into near-Earth orbit the Solar Mass Ejection Imager (SMEI) that is capable of measuring sunlight Thomson-scattered from heliospheric electrons from elongations to as close as 18° to greater than 90° from the Sun. SMEI is designed to observe time-varying heliospheric brightness of objects such as coronal mass ejections, corotating structures and shock waves. The instrument evolved from the heliospheric imaging capability demonstrated by the zodiacal light photometers of the *Helios* spacecraft. A near-Earth imager can provide up to three days warning of the arrival of a mass ejection from the Sun. In combination with other imaging instruments in deep space, or alone by making some simple assumptions about the outward flow of the solar wind, SMEI can provide a three-dimensional reconstruction of the surrounding heliospheric density structures.

Following SMEI launch early morning January 6, 2003 on the Coriolis spacecraft from Vandenberg Air Force Base, UCSD SMEI data handling and reduction technique analysis for data sets from the instrument has continued and has now been augmented throughout the period of this contract. UCSD software required to handle SMEI data files is now operating successfully in preliminary form.

We continue to accumulate SMEI data at UCSD and to analyze these data and to make them into orbital sky maps. The SMEI data UCSD receives from Sacramento Peak Observatory are backed up on DVD daily, and in addition all the data received from the Air Force are backed up onto hard drives and retained at a location removed from the UCSD campus. Data has accumulated significantly and (not funded by this contract) we continue to purchase additional terabyte hard drives as necessary to store SMEI data and the UCSD SMEI data products, and to hold these data products on-line at the UCSD campus.

SMEI data analysis continues at UCSD. During this project period we have completed processing SMEI data through to May 2008 that has included data with a camera 3 mask imposed, and have removed stars from the sky maps from these data. We have processing all of the SMEI data and have provided 3D reconstructions from these data through to the end of April 2008. Continued processing of SMEI data is expected to continue up until the end of the project period (September 30, 2008).

ACKNOWLEDGEMENTS

The work of B.V. Jackson, P.P. Hick and A. Buffington was supported in part at UCSD by this AFRL contract FA8718-04-C-0050.

Figure 1. Titan II launch of the Coriolis spacecraft on 6 January 2003 with the SMEI instrument on board.

1. INTRODUCTION

The Solar Mass Ejection Imager (SMEI) (Eyles *et al*., 2003; Jackson *et al*., 2004) was launched early on 6 January 2003 into a Sun-synchronous polar orbit from Vandenberg Air Force Base (Figure 1). The Coriolis spacecraft (Figure 2) has two instruments: an all sky imager, SMEI, and a rotating radiometer instrument, *Windsat*, intended to measure ocean winds (Gaiser *et al*., 2004).

SMEI (Keil *et al*., 1996; Jackson *et al*., 1997, 2004, and references therein) is designed to map large-scale variations in heliospheric electron densities from Earth orbit by observing Thomson-scattered sunlight from within the heliospheric volume. Conceived as an all-sky coronagraph (Jackson *et al*., 1989) SMEI views the outward flow of density structures in the solar atmosphere. These include solar coronal mass ejections (CMEs), corotating structures (streamers), and other solar wind density enhancements, or depletions such as the density variations behind shock waves. SMEI is primarily intended to demonstrate the feasibility of forecasting the arrivals of these heliospheric structures at Earth; these normally take two to five days to travel 1 AU from the Sun. To achieve this, SMEI is operated as a differential photometer with unprecedented accuracy. The instrument may be regarded as a successor to the zodiacal-light photometers (Leinert *et al*., 1975) of the twin *Helios* spacecraft and the heliospheric remote sensing capability

Figure 2. Coriolis spacecraft with the Solar Mass Ejection Imager (SMEI) instrument on board prior to Vandenberg launch. Three instrument camera baffles (circled in red) are seen on the lower portion of the spacecraft.

demonstrated by this instrument (Jackson, 1985). Such analyses make use of *in situ* solar wind data from the vicinity of the imager and extend these observations to the surrounding environment and back to the Sun. Analyses of *Helios* data (Jackson and Hick, 2002) showed that the three-dimensional (3D) location of these heliospheric density structures can be determined using tomographic modeling techniques that estimate their distance in each direction using their line-of-sight (LOS) rearrangement and brightness change caused by outward solar wind flow.

This article discusses the progress in data analysis with the SMEI instrument. Section 2 gives the signal levels expected from various heliospheric structures as derived from first-principle analyses, and Helios and SMEI observations. Section 3 describes and refers to the data handling analysis designed and being implemented to deal with SMEI data at UCSD. Section 4 shows samples of the SMEI analysis to date.

2. SMEI SIGNAL LEVELS AND DATA REQUIREMENTS

Because the Sun is much brighter than the faint coronal structures we wish to detect, SMEI was designed to carefully control the stray light background to provide a photometric sky signal that does not vary significantly over the same time intervals as the heliospheric structures being measured. Table 1 gives estimates of the signal levels expected for various phenomena at 1 AU.

TABLE 1. Expected Signal Levels

Structure	Elongation (degrees)	Signal Intensity (S10)*	Signal Duration (days)
Bright CME	60	2	1.5
	90	1	1.5
Bright Streamer	60	2	1
	90	1	1
Bright Shock	90	0.5 to 1	≤0.5
Major unidentified	60	3	2
in situ fluctuation	90	2	2
Comet Shock	20	3 to 10	-

*Signal levels are given in units of "S10" which is the surface brightness equivalent to the flux of a single tenth magnitude solar-type star per square degree of sky.

In Table 1 the brightness for coronal mass ejections (CMEs) and streamers is derived traced outward from structures using the Naval Research Laboratory's SOLWIND (Sheeley *et al*., 1980), and the High Altitude Observatory SMM coronagraphs (MacQueen *et al*., 1980), and the *Helios* photometers (Jackson, 1991).

Shock brightness was estimated from the *in situ* plasma density enhancements behind shocks observed from the *Helios* spacecraft. The values were adjusted to1 AU by assuming their brightness decreases as R^{-3} from the locations where they were actually observed closer to the Sun (Jackson, 1986). The comet shock estimates are from Jackson and Benensohn (1990).

Thomson-scattered light must be separated from many other sources of diffuse light: background light from the Sun, Moon or Earth scattered into the SMEI field of view; zodiacal light; and starlight, either individually as bright point sources or collectively as a mottled contribution to the diffuse sky brightness. Figure 3 shows estimates of the brightness contributions from these signals expected at SMEI as a function of elongation from the Sun. The Sun is the equivalent of 4×10^{14} S10 units at 1 AU. A fundamental limit to diffuse-light photometry is set by photon counting statistics; a good instrument design reduces other noise sources to this level. This limit depends upon the optics and scanning configuration, spectral bandpass, and detector efficiency. Total detected photon count N (*e.g*., Jackson *et al*., 1989) is:

$$\log_{10} N = 6.15 - 0.4m + \log_{10} A\cos\theta + \log_{10} (\Delta t), \qquad (1)$$

where A is the aperture area (cm^2), θ the incident-light angle relative to the aperture normal, Δt the integration time (seconds), and m the brightness "magnitude" in a square degree evaluated for the instrument's particular bandpass. Here, the constant 6.15 includes the bandpass efficiency for the combination of SMEI CCD and optics. For SMEI, the background sky brightness varies roughly over the range 60-6000 S10 units between the darkest sky and the ecliptic plane at a solar elongation of ~20°. The aperture is approximately 1×2 cm with A = 1.76 cm^2, and with $\Delta t = 4s$, approximately 1000 electrons are detected per S10. A given portion of sky is covered by a dozen or more frames in a single orbit, and a single-orbit photometric sky map combines roughly 1500 data frames from each of three cameras (see Eyles *et al*., 2003).

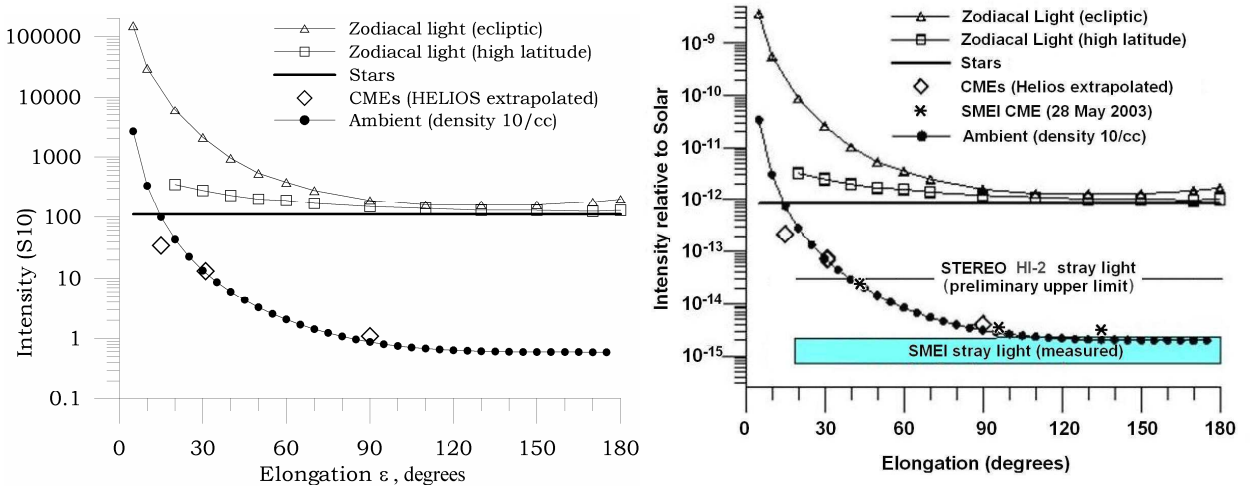

(a) **(b)**

Figure 3. Surface brightness versus solar elongation for zodiacal and starlight (Allen's Astrophysical Quantities, 2000), and of expected CME brightness extrapolated from Helios measurements. A calculation of an ambient medium having a density of 10 $e^{-}cm^{-3}$ at 1 AU and an inverse-square density dropoff with solar distance is also shown. ***a)*** *Brightness in S10, (Figure 2) at 1 AU.* ***b)*** *Brightness relative to sunlight at 1 AU. Also shown is the brightness of a large SMEI-observed CME, and the stray light levels observed in SMEI, and also that reported from the STEREO HI-2 instruments.*

The heliospheric sky brightness is large enough that CCD readout noise (~14 e^{-} rms) is not a significant factor for the SMEI camera systems when operated at the appropriate temperature. The SMEI instrument has been developed around the use of a cooled E2V CCD05-30-321A frame-transfer CCD chip, in part because this device was shown to have a satisfactory subpixel gradient response needed to reproduce stellar point images as they change position in the SMEI field of view (Buffington *et al*., 1991). To provide a reproducible photometric response with the extremely fast (~f/1) SMEI optics, unresolved point images occupy approximately 200 CCD pixels or about 1/2 square degree.

To ensure that square-degree sky locations are reproduced accurately on each orbit for the duration of heliospheric structure passage (hours to several days), the SMEI instrument requires that the response in this square degree from other sources of brightness be constant or slowly-varying to a fraction of one S10 unit. This is needed to separate heliospheric structure brightness variations from other sources of background light. Each square degree of sky contains an average of 120 S10 units of equivalent stellar signal (see Figure 3) and one star of eighth or brighter magnitude. Stellar background brightness, shown here as an average over the whole sky, varies significantly from the Milky Way to the galactic poles. Orbital motion sweeps the SMEI camera's narrow dimension over any given sidereal location in a minimum of approximately 50 seconds, and a sufficiently accurate value for stars must be recorded along with the background sky brightness despite this motion. In order that this and other bright background signals such as zodiacal light do not overwhelm the faint heliospheric signal, the differential photometric specification for these must be even better than required to eliminate stellar signals alone (see Figure 3) so that heliospheric structures are measured to a fraction of their intensities. Thus, a

differential photometric specification for all signals incident on the SMEI focal plane at 90° elongation in one square degree of sky in a single camera passage has been set at 0.1 percent.[1]

The SMEI light baffles (Figure 4) are designed so that the SMEI photometric specification can be met provided the solar limb does not approach the edge of the field of view to within 18° and 27° in the camera field-of-view's narrow and wide dimensions, respectively. When the SMEI cameras point closer than this to the Sun, the above photometric specification is unlikely to be met (Buffington *et al*., 2003) because sunlight illuminates the Z3 edge and the inner portion of the

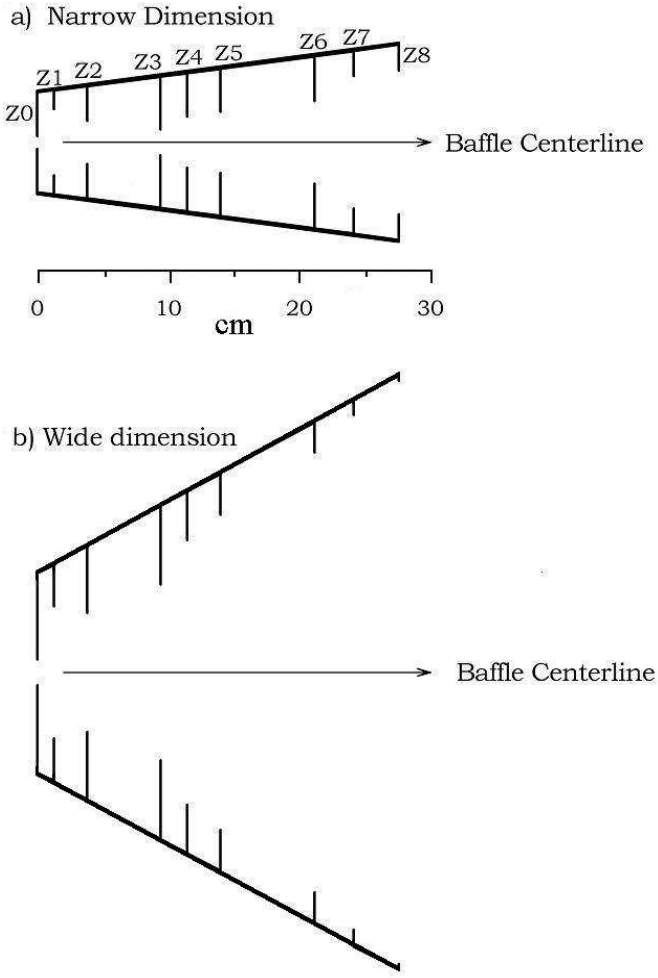

Figure 4. Schematic of SMEI baffle. The scale is in centimeters. Apertures are numbered Z0 to Z8 in advancing distance towards incident light along the baffle centerline. a) Narrow dimension. b) Wide dimension.

baffle. This portion of the baffle is imaged out of focus onto the CCD beyond the SMEI $3° \times 60°$

[1] Certain regions in the sky near bright stars, variable stars and planets exceed the 0.1 percent photometric specification. The brighter planets saturate a region of the CCD data frame near the planet. The Moon and stray light from it cause saturation of the CCD if the Moon is within 9° of the edge of the camera field of view.

field of view and when illuminated, as discovered on orbit, has sufficient brightness to saturate it with a 4s exposure. The baffle must also reject sources of background light other than the Sun, including spacecraft appendages and instrumentation, and Earthshine. Having SMEI point away from Earth controls this latter source of background light, and having SMEI also point away from the rotating (30 rpm) *Windsat* antenna (Figure 2; Figure 5) controls this potentially variable spacecraft light source. Figure 5 shows an artist's conception of the SMEI instrument in its polar orbit.

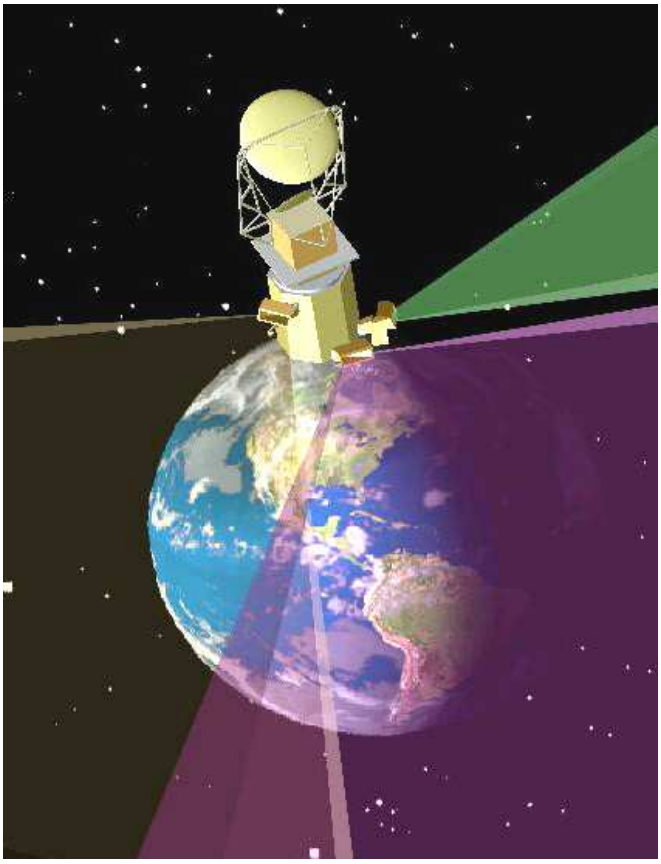

Figure 5. Schematic of SMEI in orbit. The spacecraft orbit is nearly circular at 840 km above the surface of the Earth with an inclination of 98° relative to the equatorial plane. SMEI looks outward from the Earth over an ~180° range of sky from three baffled cameras. The SMEI cameras and their fields of view as depicted are directed approximately 30° above the local horizontal to avoid both light from the Earth and sunlight reflecting from the rotating Windsat antenna (see also Figure 2).

3. SMEI DATA OPERATION AND ANALYSIS

Figure 3 shows signal levels for various phenomena at 1 AU. The proven SMEI long-term photometric performance (see Buffington *et al*., 2006a; 2007) is a 0.1% differential photometric precision, corresponding to a sky brightness of ⅓ of an S10 unit (the equivalent brightness of a 10^{th} magnitude solar-type star over a square degree of sky) in dark areas of sky and is 10^{-15} of the Sun's brightness at 1 AU.

3.1 Image Frame Processing

UCSD retrieves SMEI image frames from Sacramento Peak Observatory in near real time and maintains a database on a local server with backups on DVDs (Hick *et al*., 2005, 2007). Sacramento Peak also maintains an archive of original SMEI images. Figure 6a shows a set of simultaneous 4-second exposure 'image frames' from each of the three cameras. The Air Force Research Laboratory (AFRL) and UCSD have independently developed analysis sequences to reduce SMEI image frames to heliospheric sky maps for each orbit as in Figure 6b. These are generally displayed with an orbital time cadence of 102 minutes. The AFRL analysis sequence uses similar steps to those at UCSD, but is specifically crafted to demonstrate the feasibility of detecting and tracking solar mass ejections, and present sky maps in near real time on the Web.

The UCSD sequence of data analysis steps differs most from AFRL at the point where a high-resolution grid is formed. UCSD uses a grid of ~5 times finer angular resolution than AFRL. As this grid is formed, an algorithm removes high-energy particle hits and space debris from the data. A lesser resolution (~0.1° in latitude and longitude) sidereal sky map complete with stellar signals is then recovered from the finely divided grid for use and presentation in sidereal coordinates. A zodiacal light model, and stars are removed from these sidereal sky maps. Select locations on roughly 5-degree centers on the sky maps free of bright stars (~4000) are culled to concentrate at near-Sun locations, and are used to provide 600-orbit (40-day long) time series. From these time series, auroral signals are removed and simultaneously fit by a long-term temporal Gaussian filter with an e^{-1} weighting 200 orbits (~14 days) from the midpoint time. Higher-level data products from the 3D reconstructions using these time series are then made available on the Web at: **http://smei.ucsd.edu/** as fisheye and Hammer-Aitoff sky maps, ecliptic cuts, and remote-observer views.

3.2 SMEI Data Current Status

The UCSD SMEI analysis (Jackson *et al*., 2004) is driven by the requirement that the sky maps be as close as possible to full photometric and angular resolution design limits. This enables the best quantitative analyses; modeling heliospheric density structure using 3D reconstruction techniques is foremost here (see next subsection). SMEI sky maps should permit observing heliospheric structures that persist for a significant solar rotation fraction of a solar rotation. This enables the study of slow (corotating) as well as rapidly moving transient features. Thus, sky maps retain a constant temporal base over time periods of several weeks or longer. The 3D reconstructions require optimal removal of non-heliospheric and zodiacal artifacts, but also that minimal Thomson-scattered signal be inadvertently removed in the process.

Since light from the sidereal sky (stars, the Milky Way, nebulae, galaxies) is about 100× brighter than the variable Thomson-scattered signal (above), this background must be removed from SMEI sky maps. The simplest way to do this is by subtracting one Sun-centered sky map from the next ('running differences'); here only the change in the heliospheric signal, due to motion of the structures, over the orbital time period (Δt = 102 minutes), remains.

Tappin *et al.* (2004) use this method to study the heliospheric response to a halo CME originating on the Sun on 28 May 2003, and observed by SMEI on 29 May. In a study of SMEI data from 2003-2005 over 200 transient events were observed by SMEI (Webb *et al*., 2006), and Howard and Simnett (2008) found that most of these were first identified as CMEs in SOHO LASCO coronagraph data. Such difference maps are very sensitive to short-duration transient changes, are useful for real-time presentation of SMEI data, and are adequate for identifying and even tracking disturbances distant from Earth. However this simple analysis sacrifices the wealth of more slowly-varying features present in SMEI data. They also contain positive and negative differences, complicating both interpretation and quantitative analysis. In SMEI these analyses work well in regions free of aurora and high energy particle contamination, but suffer side effects for presentation of whole-sky SMEI images because these effects are not removed by orbit-to-orbit subtraction procedures.

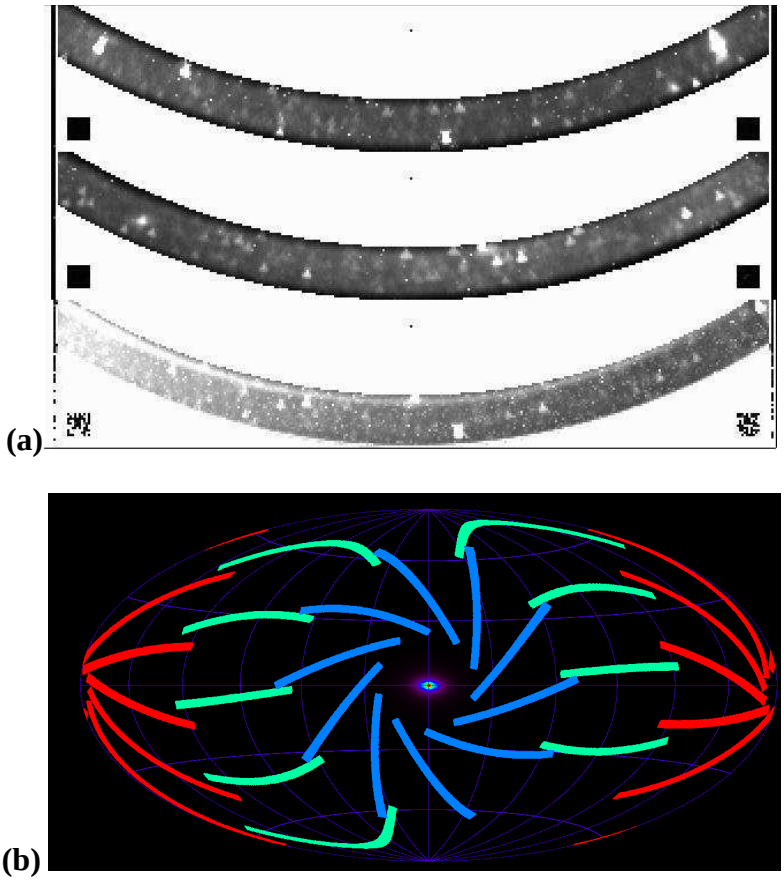

Figure 6 ***a)*** *3°×60° image frames from each of the three SMEI cameras. Camera 1 (top) views farthest from the Sun; camera 3 (bottom) closest, with the Sun towards the left in each frame.* ***b)*** *Full-sky Hammer-Aitoff projection showing the placement of a sample of SMEI camera image frames with the Sun centered in the projection (in October). About 4500 frames per orbit fill in the sky in a clockwise direction every 102 minutes. Camera 1 is shown in red, Camera 2 is in green, and Camera 3 is in blue. See:* ***http://smei.ucsd.edu*** *for the SMEI archive of images, orbit by orbit difference sky maps, and a host of higher-level data products including 3D reconstructions.*

The subtraction of a long-term base is likewise hampered in SMEI analyses by auroral brightness in some portions of the images (see Mizuno *et al*., 2004), high energy particle contamination, and some stellar stray-light bleed-in effects at the edges of each camera image. In addition, slow movement of the variable zodiacal light relative to the sidereal sky (Buffington *et al*., 2006b) adds measurement noise. Each of these contaminants is identified in computer software and has been dealt with in successive steps to provide time series that are essentially free from these. Thus, a long term base can be subtracted (see Jackson *et al*., 2004; 2006). As an example, the auroral contaminant signals appear only in certain locations in the SMEI orbit, but at differing times. These signals can thus be largely eliminated in the time series by employing an iterative edge filter that recognizes rapid

brightness onsets in the orbital and temporal domains where these signals are known to occur (see Jackson *et al*., 2007b; 2008b).

Figure 7 shows the location of the chosen sidereal LOS in a SMEI sky map (see Jackson *et al*., 2006) and Figure 8 (from Jackson *et al*., 2008b) shows such time series essentially free from these contaminants. Here we see the SMEI sidereal-background brightness changes with a long term base removed over a temporal interval that includes a bright ICME. We now have accurate SMEI calibrations that relate SMEI CCD Analog to Digital Units (ADUs) to sky brightness. For camera 2, 1 S10 = 0.46±0.02 ADU, and slightly different per camera, has been used to relate the LASCO coronagraph calibration to SMEI brightness from a set of stars observed by both (Buffington *et al*., 2007).

The calibrated time series data are the basis of many of the SMEI analyses to the present. The 3D results evaluated at in-situ spacecraft locations provide measurements that in turn refine SMEI images: the original sky maps are contaminated by troublesome backgrounds and portions of these are sometimes further swamped by bright auroral light. Extrapolating across these regions and removing contaminant signals is accomplished for SMEI data as was done (and is still done) from IPS sky maps. Here, outages and contaminant signals are modeled away using a realistic 3D solar wind model iteratively fit to the data, both removing the contaminated regions and then extrapolating across them. The final editing retains just the heliospheric signal in the sky maps.

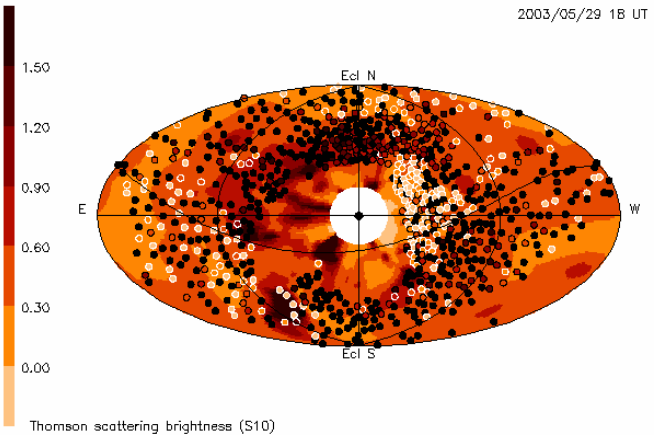

Figure 7. SMEI image depicting all of the sky as observed from Earth and including the positions of the edited lines of sight present within a day of the indicated time. The data point color indicates the relationship of the line-of-sight brightness signal at these locations relative to the brightness in the Thomson scattering reconstruction.

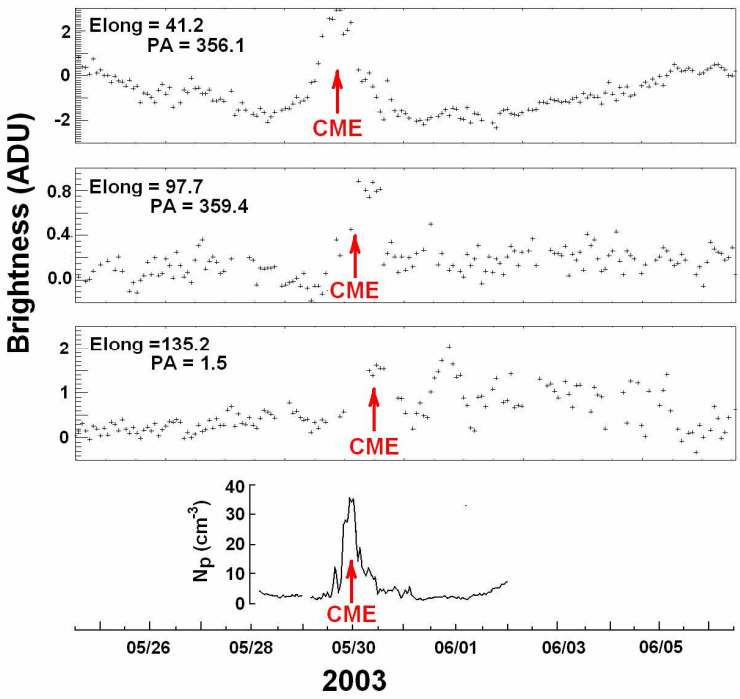

Figure 8. SMEI brightness measurements obtained during the 27-28 May 2003 halo ICME. The three upper panels show examples of time series (in ADU, at 102-minute intervals) from three individual square degrees of sky at different angular distances from the Sun, after removing a long-term base. The lower panel shows one-hour average proton density from ACE level 0 data.

4. SAMPLES OF THE SMEI ANALYSIS

4.1 UCSD Heliospheric 3D Reconstruction

The 3D reconstruction technique has been developed since the early 1990's as a way to precisely measure 3D heliospheric structures and to forecast ICME and corotating structure Earth-arrival. A short synopsis of this can be found on the UCSD SMEI Website at: **http://smei.ucsd.edu/imageinfo.html**/ with more explanation in Jackson *et al*. (1998; 2006; 2007b, 2008b); Kojima *et al*. (1998); Jackson and Hick (2002; 2005); and Hick and Jackson (2004). The basic concept: reconstructions proceed by fitting a heliospheric solar wind model to observed brightness using well-established Thomson-scattering parameters (Billings, 1966). Perspective views of these structures are provided by the outward solar wind flow that changes the LOS aspect of the structures passing the observer. Prior to SMEI these computer-aided tomography (CAT) techniques were successfully applied to HELIOS spacecraft photometer brightness (Jackson *et al*., 2001; Jackson and Hick, 2002) and to IPS remote sensing data from the STELab radio arrays. Although the scattering process for IPS differs from Thomson scattering (see Jackson and Hick, 2005), the mathematical description is similar enough that the 3D reconstruction procedure proceeds in essentially the same way for both data sets.

Presently, the reconstruction incorporates a purely kinematic solar wind model. Given the velocity and density of an inner boundary (the 'source surface'), a fully 3D solar wind model best fitting the observations is calculated by assuming radial outflow and enforcing conservation of mass and mass flux outward from this boundary (Jackson *et al*., 1998). Best fit is achieved iteratively: when the LOS integrations of 3D solar wind at large solar distance do not match the overall observations, the source surface values are altered (inverted tomographically) and the deviations reduced. Extensive study has shown that the final iterated values are insensitive to the starting values on the source surface, and that most of the convergence occurs within one or two iterations (Jackson *et al*., 2008b).

This technique analyzes ICME-associated structures using IPS and SMEI Thomson-scattering observations. Figure 9a is an ecliptic cut example of a 3D heliospheric analysis using SMEI Thomson scattering brightness and STELab IPS velocity data with digital time steps of ½ day and resolutions in latitude and longitude of 6.7°. Different Gaussian filters are used for the two data sets to limit the observed structure size to larger than the digital resolution (Jackson and Hick, 2005; Jackson *et al*., 2006; 2008b). Figure 9b compares the 3D reconstruction with Wind spacecraft plasma density data and Figure 9c shows the correlations between these (from Jackson *et al*., 2008b).

Unlike the IPS analyses, the SMEI density reconstruction must include an unknown steady brighter background component from the ambient solar wind. An estimate for this is provided by *in situ* observations near Earth. The steady-state part of the ambient solar wind is a measurable component *in situ* and its brightness is on top of other steady brightness such as that from the zodiacal cloud. In the 30 May 2003 example, the background density is observed to be approximately 4 protons cm^{-3} (see Figure 9b). This is a small proportion of the total attributed to the ICME density (or mass) in this instance. A comparison to *in situ* proton densities also requires that a correction be made for the helium abundance here assumed to be 10% throughout the remotely-observed ICME structure, an equivalent 20% more electrons and thus 1 S10 becomes 0.552 ADU. Large events often have significant differences in the proton number at different *in situ* spacecraft monitors, and the SMEI analyses are now often good enough to distinguish which instrument or instruments give an appropriate measurement.

The above analysis of this event compares well with other models of his event, most notably the HAF kinematic model (Sun *et al*., 2008). Because we now analyze these ICME events fully in 3D, we have also measured their interplanetary mass and energy (Figure 10), and compared these to equivalent LASCO coronagraph values. For the 27-28 May 2003 events observed in LASCO, the ICME response measured by SMEI is a composite of several halo CMEs that arrive at Earth at approximately the same time. We measure several components of these events and trace them outward from the Sun where their comparisons give very similar mass once a correction for the distance from the plane of the sky is applied to the

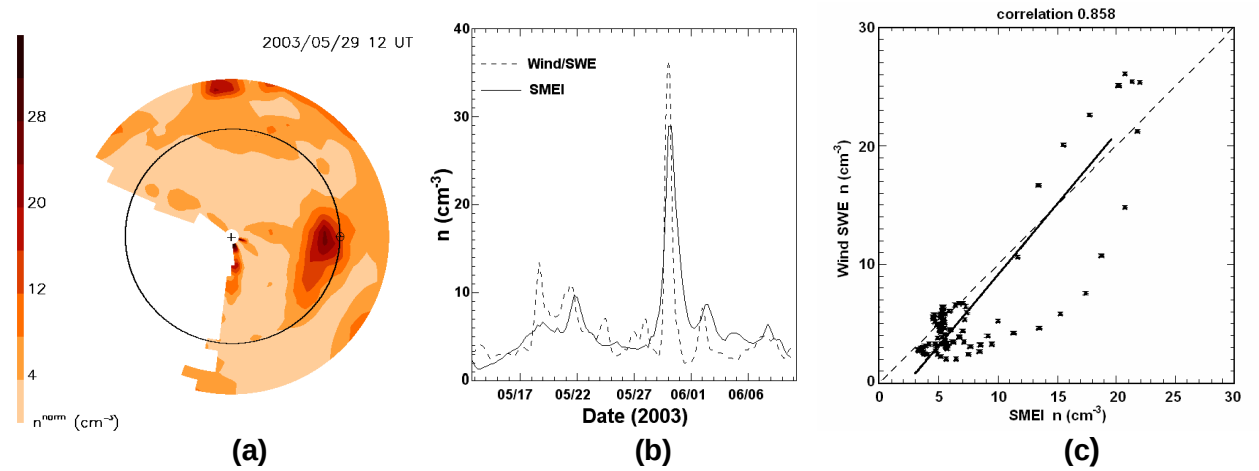

Figure 9. 3D density reconstruction of the 27-28 May halo CME sequence of events as it reaches Earth (as in Jackson et al., 2008b). ***a)*** *An ecliptic plane cut of the measurements at the time indicated. The Sun is at the center, Earth is right in the image, the density scale is left. An* r^{-2} *density fall-off has been removed so that the densities shown scale to 1 AU. Angular resolution is 6.7º × 6.7º in latitude and longitude. The temporal cadence is ½ day. The main structure at Earth is associated with the halo CME sequence observed by LASCO on 27-28 May 2003, and shows that the density enhancement of the CME that hits Earth in this event is more extensive to the East of the Sun than to the West.* ***b)*** *Time series plot of the density at Earth from the reconstruction and from Wind proton observations for the whole Carrington rotation that includes the CME. The latter in situ observations are combined into 18-hour averages matching the temporal and spatial resolutions of the low-resolution SMEI reconstruction.* ***c)*** *Correlation of the reconstruction with the Wind data. The correlation is limited to within 6 days of the event (Jackson et al., 2008b).*

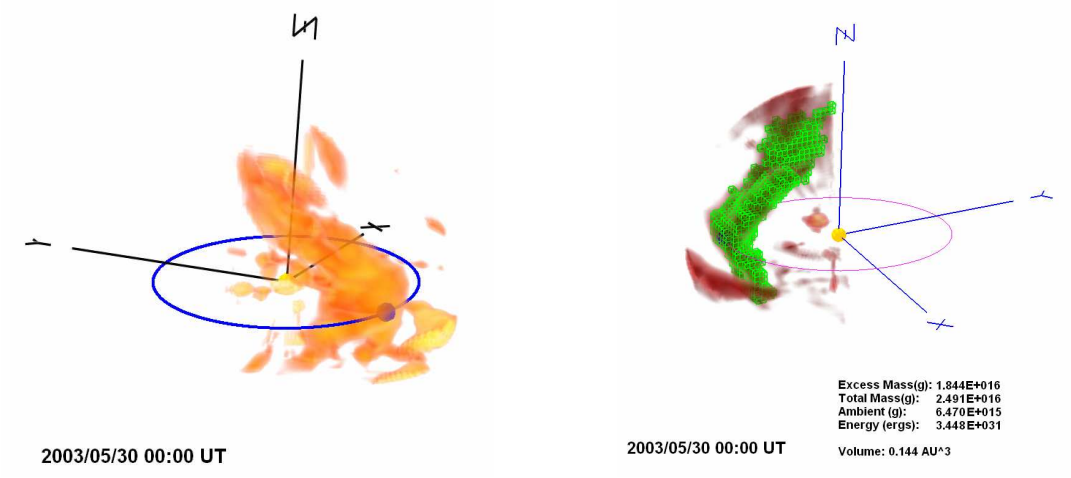

Figure 10. 3D mass determination for the 27-28 May 2003 halo CME sequence as the associated ICMEs reach Earth vicinity at 00:00 UT 30 May 2003. Electron density is contoured upward from 15 cm^{-3}. ***a)*** *The ICME observed from about 45º East of the Sun-Earth line and 20º above the ecliptic plane just as the event sequence begins to engulf the Earth.* ***b)*** *The total event is highlighted and filled with cubes, has a volume of 0.144* AU^3 *above this contour interval, and a total mass of* 2.49×10^{16} *g.*

coronagraph observations. The total mass of the composite ICME above is larger but within a factor of two, of the total excess mass measured by the LASCO coronagraph for all of the events in the sequence that comprise the ICME. Kinetic energies of the ICME outward motion amount to 3.4×10^{31} erg for this event sequence.

Figure 11 shows an ecliptic cut presentation of the 3D reconstruction of the 28 October 2003 "Halloween Storm" CME, a recent SHINE workshop "campaign event" using SMEI observations (Jackson *et al*., 2006). This CME was observed by both the STELab IPS and SMEI about the same time, and both analyses yield approximately the same total mass for the northward ICME portion (Tokumaru *et al*., 2007; Jackson *et al*., 2007a). Many studies have been made of this event, often in association with space weather and the SHINE workshops, but the SMEI heliospheric analyses are unique. The shock response for this event arrived at Earth ~20 hours after its first visibility on the Sun (Cliver and Svalgaard, 2004). It was associated with a large geomagnetic storm, followed by the passage of a geomagnetic cloud and flux cylinder elongated in approximately the same direction as the dense region observed by the IPS and SMEI. The dense material traveling from Sun to Earth on average at ~800 km s^{-1} was present only in the trailing portion of the flux cylinder (Jensen *et al*., 2006), and these ejecta stretched from the northern to southern hemisphere on the Sun and arose from a slow solar wind region in the corona (Jackson *et al*., 2006; Tokumaru *et al*., 2007).

During this last year a breakthrough in our 3D reconstruction for SMEI data has improved resolution, and our reconstructions now show not only the dense central core associated with this large ICME, but also the density enhancement in front of the ICME shock. In Figure 11, a planar ecliptic cut through this event shows a curved high density front that we attribute to a sheath-shock density enhancement preceding the event into the heliosphere. The shock sheath is not continuous nor does it form a uniform front ahead of the ICME in our analyses. If it were, ample SMEI data would show it at these other locations. Although this reconstructed shock is observed for one of the largest CMEs on record, we now see many similar small curved structures in higher-resolution SMEI analyses, and we have connected these to *in situ* measurements at Earth and at the STEREO spacecraft during the current era and have confirmed that they are indeed often associated with shock density enhancements.

4.2 Future UCSD Analysis

Future analyses should allow all of these features to be studied in 3D and measured as density so that they can be interpreted and forecast in a more comprehensive way, for instance as we do currently with IPS data (see **http://ips.ucsd.edu**). To do this at the best resolutions possible will require use of the whole image data set (instead of using only approximately 1/50th of the data as shown in Figure 7). This is not possible to automate to the fine limits set by the current UCSD indexing program without considerable effort, since the system from the start was never designed to be run in real time. Tomography using the full data set and this same reconstruction technique requires a parallel processor and the 3D reconstruction programmed in such a system. Although we now have a preliminary version of our 3D reconstruction program running on the NASA Ames Research Center Columbia parallel processor, more work is needed to provide the most up-to-date analysis techniques for SMEI use for retrospective analysis using supercomputer systems.

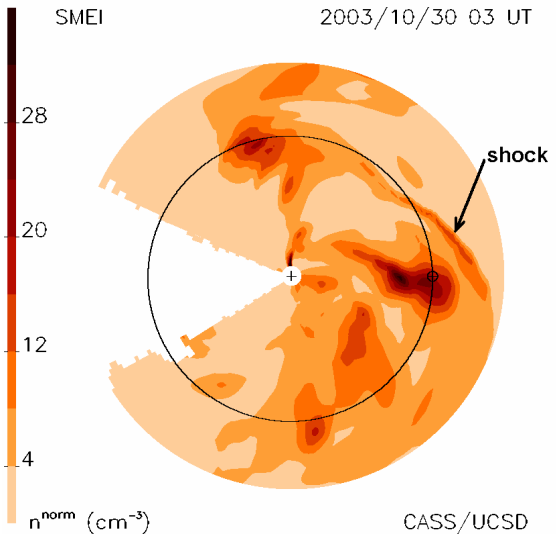

Fig. 11. SMEI-derived density ecliptic cut showing the 3D reconstruction of the density enhancement behind a shock.

Journal articles/presentations partially supported by this contract

Those references marked by *

REFERENCES:

Billings, D.E., 1966, 'A guide to the solar corona', Academic, New York, p. 150.

*Bisi, M.M., Jackson, B.V., Hick, P.P., and Buffington, A., 2007a, 'CME Reconstructions Using Interplanetary Scintillation Data', presented at the at the Living With a Star Geostorm CDAW and Conference, Florida Inst. of Technology, Melbourne, FL, March 8, 2007.

*Bisi, M.M., Jackson, B.V., Buffington, A., Manoharan, P.K., Fallows, R.A., Kojima, M., Tokumaru, M., Breen, A.R., Hick, P.P., Dorrian, G.D., Clover, J.M., and Buffington, A., 2007c, '3D Reconstructions Using Interplanetary Scintillation (IPS) and the Solar Mass Ejection Imager (SMEI) Data', presentation at the CAWSES Workshop, Kyoto, Japan 23-27 October, 2007.

*Bisi, M.M., Jackson, B.V, and Clover, J.M., 2007d, 'SMEI – IPS – Ulysses – STEREO: Current UCSD Comparison Progress', presentation at the Toyokawa IPS Workshop, Toyokawa, Japan, 30-31 October, 2007.

*Bisi, M.M., Jackson, B.V., Breen, A.R., Fallows, R.A., Feynman, J., Clover, J.M., Hick, P.P., and Buffington, A., 2007e, 'IPS Observations of the Inner-Heliosphere and their Comparison with Multi-Point In-situ Measurements', poster at the AGU (American Geophysical Union) Fall Meeting, San Francisco, CA, U.S.A., December 2007.

*Bisi, M.M., Jackson, B.V., Hick, P.P., Buffington, A., and Clover, J.M., 2008a, 'Coronal mass ejection reconstructions from interplanetary scintillation data using a kinematic model: a brief review', Chapter 12, 4th Asia-Oceania Geophysical Society General Assembly Proceedings, Advances in Geosciences (in press).

*Bisi, M.M., Jackson, B.V., Hick, P.P., Buffington, A., and Clover, J.M., 2008b '3D Reconstructions of the Early November 2004 CDAW Geomagnetic Storms: Preliminary analysis of STELab IPS speed and SMEI density', *J. Geophys Res.* (in press).

*Bisi, M.M., Jackson, B.V., Buffington, A., Hick, P.P., Manoharan, P.K., and Clover, J.M., 2008c, 'Solar Wind and CME Reconstructions in the Inner Heliosphere', solicited presentation at the 5th Asia Oceania Geophysical Society General Assembly, Busan, South Korea, June 2008.

*Bisi, M.M., Jackson, B.V., Hick, P.P., Buffington, A., and Clover, J.M., 2008d, '3D Reconstructions of the Inner Heliosphere', poster at the SHINE-GEM Meeting, Midway, UT, U.S.A., June 2008.

*Bisi, M.M., Jackson, B.V., Buffington, A., Hick, P.P., Manoharan, P.K., and Clover, J.M., 2008e, 'Solar Wind and CME Reconstructions in the Inner Heliosphere', 5th Asia-Oceania

Geophysical Society General Assembly Proceedings, *Advances in Geosciences*, submitted 10 September 2008.

Buffington, A., Booth, C.S. and Hudson, H.S., 1991, 'Using Image Size to Control Systematic Error in CCDs', *PASP* **103**, 685.

Buffington, A., Jackson, B.V., and Hick, P.P.: 2003, 'Calculations for, and laboratory measurements of a multistage labyrinthine baffle for SMEI in: Keil, S.L., and Avakyan, S.V., (eds.), 'Innovative Telescopes and Instrumentation for Solar Astrophysics', Proc. SPIE **4853**, 490−503.

*Buffington, A., Band, D.L., Jackson, B.V., Hick, P.P., and Smith, A.C., 2006a, 'A Search for Early Optical Emission at Gamma-Ray Burst Locations by the Solar Mass Ejection Imager (SMEI)', *Astrophys. J*. **637,** 880.

*Buffington, A., Jackson, B.V., Hick, P. and Price, S.D., 2006b, 'An Empirical Description of Zodiacal Light as Measured by SMEI', *EOS Trans*. *AGU* **87(52)**, Fall Meet. Suppl., Abstract, SH32A-06.

*Buffington, A., Morrill, J.S., Hick, P.P., Howard, R.A., Jackson, B.V., and Webb. D.F., 2007, 'Analysis of the Comparative Responses of SMEI and LASCO', in *Proc. SPIE* **6689**, 66890B, 1-10.

Cliver, E.W., and Svalgaard, L., 2004, 'The 1859 solar-terrestrial disturbance and the current limits of extreme space weather activity', *Solar Phys*. **224**, 407.

Eyles, C.J., Simnett, G.M., Cooke, M.P., Jackson, B.V., Buffington, A., Hick, P.P., Waltham, N.R., King, J.M., Anderson, P.A., and Holladay, P.E., 2003, 'The Solar Mass Ejection Imager (SMEI)', *Solar Phys.*, **217**, 319.

Gaiser, P.W., St. Germain, K.M., Twarog, M., Poe, G.A., Purdy, W., Richardson, D., Grossman, W., Jones, W.L., Spencer, D., Golba, G. Clevland, J., Choy, L., Bevilacqua, R.M., Chang, P.S., 2004, 'The WindSat space borne polarimetric microwave radiometer: sensor description and early orbit performance", *IEEE Trans. On Geosci. And Remote Sensing, 42 (11),* 2347.

*Harra, L.K., Crooker, N.U., Mandrini, C.H., van Driel-Gesztelyi, L., Dasso, S., Wang, J., Elliott, H., Attril, G., Jackson, B.V., Bisi, M.M., 2008, 'How does large flaring activity from the same active region produce oppositely directed magnetic clouds?', *Solar Phys*., **244**, 95-114.

Hick, P.P., and Jackson, B.V., 2004, 'Heliospheric tomography: an algorithm for the reconstruction of the 3D solar wind from remote sensing observations', *Proc. SPIE* **5171**, 287-297.

Hick, P.P., Buffington, A., and Jackson, B.V., 2005, 'The SMEI real-time data pipeline: From raw CCD frames to photometrically accurate full-sky maps', *Proc. SPIE,* **59011B**, doi: 10.1117/12.617996.

Hick, P.P., Buffington, A., and Jackson, B.V. 2007, 'A Procedure for Fitting Point Sources in SMEI White-Light Full-Sky Maps', in *Proc. SPIE* **6689,** 66890C, 1-8.

Howard, T.A., and Simnett, G.M., 2008, 'Interplanetary coronal mass ejections that are undetected by solar coronagraphs', *J. Geophys. Res*. **113**, A08102.

Jackson, B.V., 1985, 'Imaging of Coronal Mass Ejections by the Helios Spacecraft', *Solar Phys*. **100**, 563.

Jackson, B.V.: 1986, 'Helios photometer measurement of in situ density enhancements', *Adv. Space Res*. **6**, 307.

Jackson, B.V., 1991, 'Helios Spacecraft Photometer Observations of Elongated Corotating Structures in the Interplanetary Medium', *J. Geophys. Res*. **96**, 11,307.

Jackson, B.V., and Benensohn, R.M., 1990, 'The Helios spacecraft zodiacal light photometers used for comet observations and views of the Comet West bow shock', *Earth, Moon and Planets* **48**, 139.

Jackson, B.V., and Hick, P.P., 2002, 'Corotational tomography of heliospheric features using global Thomson scattering data', *Solar Phys*. **211**, 344.

*Jackson, B.V., and Hick, P.P., 2005, 'Three-dimensional tomography of interplanetary disturbances', Chapter 17 in: D.E. Gary, and C.U. Keller (eds.), *Solar and Space Weather Radiophysics, Current Status and Future Developments*, Astrophysics and Space Science Library, **Vol. 314**, p. 355-386, Kluwer Academic Publ., Dordrecht, The Netherlands, 2005.

Jackson, B.V., Hudson, H.S., Nichols J.D., and Gold, R.E., 1989, 'Design Considerations for a "Solar Mass Ejection Imager" on a Rotating Spacecraft', in *Solar System Plasma Physics Geophysical Monograph*, **54**, J.H. Waite, Jr, J.L. Burch and R.L. Moore, eds., 291.

Jackson, B.V., Buffington, A., Hick, P.L., Kahler, S.W., Simnett, G. and Webb, D.F., 1997b, 'The solar mass ejection imager', *Physics and Chemistry of the Earth*, **22**, No. 5, 441.

Jackson, B.V., Hick, P.L., Kojima, M., and Yokobe, A., 1998, 'Heliospheric Tomography Using Interplanetary Scintillation Observations 1. Combined Nagoya and Cambridge data', *J. Geophys. Res*. **103**, 12,049.

Jackson, B.V., Buffington, A., and Hick, P.P., 2001, 'A heliospheric imager for Solar Orbiter', Proc. 'Solar Encounter: The First Solar Orbiter Workshop', May 14-18, 2001, Santa Cruz de Tenerife, Spain, *ESA SP*-**493**, 251.

Jackson, B.V., Hick, P.P., and Buffington, A., 2002, 'Time-dependent tomography of heliospheric features using the three-dimensional reconstruction techniques developed for the Solar Mass Ejection Imager (SMEI)', *Proc. SPIE, Waikoloa*, 22-28 August 2002, **4853**, 23.

*Jackson, B.V., Buffington, A., Hick, P.P., Altrock, R.C., Figueroa, S., Holladay, P.E., Johnston, J.C., Kahler, S.W., Mozer, J.B., Price, S., Radick, R.R., Sagalyn, R., Sinclair, D., Simnett, G.M., Eyles, C.J., Cooke, M.P., Tappin, S.J., Kuchar, T., Mizuno, D., Webb, D.F., Anderson, P.A., Keil, S.L., Gold, R.E., and Waltham, N.R., 2004, 'The Solar Mass Ejection Imager (SMEI) Mission', *Solar Phys*. **225**, 177-207.

*Jackson, B. V., Buffington, A., Hick, P.P., Wang, X. and Webb, D., 2006, 'Preliminary three-dimensional analysis of the heliospheric response to the 28 October 2003 CME using SMEI white-light observations', *J. Geophys. Res.* **111, A4**, A04S91.

*Jackson, B.V., Hick, P.P., Buffington, A., Bisi, M.M., Kojima, M., and Tokumaru, M., 2007a, 'Comparison of the extent and mass of CME events in the interplanetary medium using IPS and SMEI Thomson scattering observations', in I. Chashei, and V. Shishov, eds. Scattering and Scintillation in Radio Astronomy, *Astronomical and Astrophysical Transactions*, **26:6**, 477-487 doi:10.1080/10556790701612221.

*Jackson, B.V., Buffington, A., Hick, P.P., Bisi, M.M., and Jensen, E.A., 2007b, 'SMEI Observations in the STEREO Era', in *Proc. SPIE* **6689**, 66890C, 1-8.

*Jackson, B.V., Hick, P.P., Bisi, M.M., Buffington, A., and Clover, J.M., 2008a, 'The UCSD Solar Mass Ejection Imager (SMEI) and Interplanetary Scintillation (IPS) Web Database, and CCMC Models', SHINE 08 Workshop, Zermatt, Utah, 23- 27 June, 2008.

*Jackson, B.V., Bisi, M.M., Hick, P.P., Buffington, A., Clover, J.M., and Sun, W., 2008b, 'Solar Mass Ejection Imager (SMEI) 3D reconstruction of the 27-28 May 2003 CME sequence', *J. Geophys Res*., (in press).

Jensen, E.A., Mulligan, T., Jackson, B.V., and Tokumaru, M., 2006, '3-D Magnetic Field Geometry of the October 28, 2003 ICME: Comparison with SMEI White-Light Observations', EOS Trans. AGU 87(52), Fall Meet. Suppl., Abstract SH33A-0397.

Keil, S.L, Altrock, R.C., Kahler, S.W., Jackson, B.V., Buffington, A., Hick, P.L., Simnett, G., Eyles, C., Webb, D.F., and Anderson, P., 1996, 'The Solar Mass Ejection Imager (SMEI)', Denver 96 "Missions to The Sun", *SPIE* **2804**, 78.

Kojima, M., Tokumaru, M., Watanabe, H., Yokobe, A., Asai, K., Jackson, B.V., and Hick, P.L., 1998, 'Heliospheric Tomography Using Interplanetary Scintillation Observations 2. Latitude and Heliocentric Distance Dependence of Solar Wind Structure at 0.1-1 AU', *J. Geophys. Res*. **103**, 1981.

Leinert, C., Link, H., Pitz, E., Salm, N., and Knuppelberg, D.: 1975, *Raumfahartforschung* **19**, 264.

MacQueen, R.M., Csoeke-Poeckh, A., Hildner, E., House, L., Reynolds, R., Stanger, A., Tepoel, H., and Wagner, W.: 1980, *Solar Phys*. **65**, 91.

Mizuno, D.R., Buffington, A., Cooke, M.P., Eyles, C.J., Hick, P.P., Holladay, P.E., Jackson, B.V., Johnston, J.C., Kuchar, Mozer, J.B., Price, S., Radick, R.R., Simnett, G.M., Sinclair, D., and Webb, D.F., 2004, 'Very High-Altitude Aurora Observations With the Solar Mass Ejection Imager', *J. Geophys. Res.*, (submitted).

Sheeley, N.R., Jr., Michels, D.J., Howard, R.A., and Koomen, M.J.: 1980, *Astrophys. J*. **237**, L99.

Sun, W., Deehr, C.S., Dryer, M., Fry, C.D., Smith, Z.K., and Akasofu, S.-I., 2008, 'Simulated SMEI and "STEREO-like views" of the Solar Wind following Solar Flares on 27-29 May 2003', Space Weather, **6**, S03006, doi:10.1029/2006SW000298.

Tappin, S.J., Buffington, A., Cooke, M.P., Eyles, C.J., Hick, P.P., Holladay, P.E., Jackson, B.V., Johnston, J.C., Kuchar, T., Mizuno, D., Mozer, J.B., Price, S., Radick, R.R., Simnett, G.M., Sinclair, D., Waltham, N.R., and Webb, D.F., 2004, 'Tracking a major interplanetary disturbance with SMEI', *Geophys. Res. Lett.* **31**, L02802.

*Tokumaru, M., Kojima, M., Fujiki, K., Yamashita, M., and Jackson, B.V., 2007, 'The source and propagation of the interplanetary disturbance associated with the full-halo coronal mass ejection on 2003 October 28', *J. Geophys. Res*. **112**, A05106, doi:10.1029/2006JA012043.

*Webb, D.F., Mizuno, D.F., Buffington, A., Cooke, M.P., Eyles, C.J., Fry, C.D., Gentile, L.C., Hick, P.P., Holladay, P.E., Howard, T.A., Hewitt, J.G., Jackson, B.V., Johnston, J.C., Kuchar, T.A., Mozer, J.B., Price, S., Radick, R.R., Simnett, G.M., and Tappin, S.J., 2006, 'Solar Mass Ejection Imager (SMEI) Observations of CMEs in the Heliosphere', *J. Geophys. Res*., **111**, A12101, doi:10.1029/2006JA011655.